Supplementary Materials

Maximized Ir atom utilization via downsizing active sites to single-atom scale for highly stable dry reforming of methane

Yangyang Li[1,2], Cun Liu[1,*], Yang Su[1], Yang Zhao[3], Botao Qiao[1,*]

[1]CAS Key Laboratory of Science and Technology on Applied Catalysis, Dalian Institute of Chemical Physics, Chinese Academy of Sciences, Dalian 116023, Liaoning, China.
[2]University of Chinese Academy of Sciences, Beijing 100049, China.
[3]Dalian National Laboratory for Clean Energy, Dalian Institute of Chemical Physics, Chinese Academy of Sciences, Dalian 116023, Liaoning, China.

[*]**Correspondence to:** Prof. Botao Qiao, Dr. Cun Liu, CAS Key Laboratory of Science and Technology on Applied Catalysis, Dalian Institute of Chemical Physics, Chinese Academy Sciences, No. 457 Zhongshan Road, Dalian 116023, Liaoning, China.
E-mail: bqiao@dicp.ac.cn; liucun@dicp.ac.cn

Derivation of the Dispersion Formula

For spherical particles, useful relationships between metal dispersion, surface area and mean particle diameter can be established by making assumptions on the nature of the crystal planes exposed on the metal surface. Thus, assuming equal proportions of the three low-index planes (111), (100) and (110) on the polycrystalline surface of a face-centered cubic (fcc) metal, it is easy to calculate, from crystal data, the number of atoms per unit area in these planes and the mean number of atoms n_s. The surface area a_m occupied by an atom m on a polycrystalline surface is $a_m = 1/n_s$. The volume v_m occupied by an atom m in the bulk of metal is given by

$$\nu_m = \frac{M}{\rho \cdot N_A},$$

where M is the atomic mass, ρ the mass density and N_A Avogadro's number (6.022 × 1,023 mol^{-1}). In the case of iridium (M = 192.2 $g \cdot mol^{-1}$; ρ = 22.42 $g \cdot cm^{-3}$).

The relationship between specific surface area (S_{sp}) and dispersion (D) is

$$S_{sp} = a_m \left(\frac{N_A}{M} \right) D,$$

The relationship between specific surface area (S_{sp}) and mean particle size (d_{VA}) is

$$S_{sp} = \frac{\Sigma n_i A_i}{\rho_i \Sigma n_i V_i},$$

Since $A_i = \pi d_i^2$ and $V_i = \pi d_i^3 / 6$, S_{sp} is given by

$$S_{sp} = \left(\frac{6}{\rho} \right) \frac{\Sigma n_i d_i^2}{\Sigma n_i d_i^3},$$

And since $d_{VA} = \frac{\Sigma n_i d_i^3}{\Sigma n_i d_i^2}$, $S_{sp} = \frac{6}{\rho \cdot d_{VA}},$

With d_{VA} expressed in nanometers, ρ in $g \cdot cm^{-3}$ and S_{sp} in $m^2 \cdot g^{-1}$, this becomes

$$S_{sp} = \frac{6000}{\rho \cdot d_{VA}},$$

The relationship between metal dispersion (D) and mean particle size (d_{VA}) is

$$d_{VA} = 6\left(\frac{\Sigma n_i V_i}{\Sigma n_i A_i}\right) = 6\left(\frac{v_m N_T}{a_m N_S}\right),$$

Since $N_S/N_T = D$, then $D = 6\dfrac{(v_m/a_m)}{d_{VA}}$.

As for iridium, a_m=7.73 /Å^2, $v_m = 14.24$ /Å^3, so $D = \dfrac{1.1053}{d_{VA}}$, where the mean particle size [d_{VA} (nm)] was statistically derived from electron microscopy images.

Supplementary Figures

Supplementary Table 1. Design of experiments on the external diffusion

Catalyst amount (mg)[a]	Flow velocity (mL/min)	Liner velocity (cm/min)
10	6	7.89
20	12	15.79
30	18	23.68
50	30	39.47
70	42	55.26
100	60	78.95

[a]The catalyst was diluted with 70-80 mesh quartz sand to ensure a fixed bed height-to-diameter ratio exceeding 2.5.

Supplementary Table 2. The BET surface areas and iridium loadings based on ICP-OES of x% Ir/TiO$_2$

Sample	Ir loading (%)	BET area (m^2/g)
TiO$_2$	-	46.50
0.01% Ir/TiO$_2$	0.0057	40.38
0.05% Ir/TiO$_2$	0.0305	39.43
0.2% Ir/TiO$_2$	0.1426	36.74
0.5% Ir/TiO$_2$-batch 1	0.3496	40.78
0.5% Ir/TiO$_2$-batch 2	0.3490	-
0.5% Ir/TiO$_2$-batch 3	0.3425	-
1.0% Ir/TiO$_2$	0.7888	40.26

Supplementary Table 3. Irk L_3-edge EXAFS fitting results for as-prepared catalysts

Sample	Shell	R (Å)[a]	C.N.[b]	σ^2 ((Å)[c]	E_0 shift (eV)	R-factor
Ir foil	Ir-Ir	2.71	12	0.00403	8.888	0.0151
IrO$_2$	Ir-O	1.98	6	0.00384	12.481	0.0077
	Ir-Ir	3.14	6	0.00707	12.481	
sample1	Ir-O	2.03	4.73	0.00594	13.813	0.0294
sample2	Ir-O	2.03	4.5	0.00769	13.505	0.0104
	Ir-Ir	2.73	1.35	0.00075		
sample3	Ir-O	2.03	3.67	0.00717	15.758	0.0088
	Ir-Ir	2.73	2	0.00258		
	Ir-Ir	3.22	7.86	0.02459		
sample4	Ir-O	2.02	2.9	0.00837	13.956	0.0185
	Ir-Ir	2.72	2.79	0.00321		

[a]R is interatomic distance (the bond length between Ir central atoms and surrounding coordination atoms).
[b]C.N. is the coordination number.
[c]σ^2 is Debye-Waller factor (a measure of thermal and static disorder in absorber scatter distances).
[d]E_0 shift is edge energy shift (the difference between the zero kinetic energy value of the sample and that of the theoretical model).

Supplementary Table 4. Kinetic Activity Assessment and Turnover Frequency (TOF) Determination

Sample	Catalyst amount (mg)	Temperature (°C)	Flow rate (mL/min)	Conversion (%)[a]	
				CH_4	CO_2
0.01 % Ir-TiO$_2$	50.1	700	15.00	7.9597 (±0.02)	13.2794 (±0.04)
		750	30.00	10.6188 (±0.05)	20.1961(±0.32)
0.05 % Ir-TiO$_2$	10.6	700	15.00	7.8396 (±0.15)	13.0286 (±0.36)
		750	50.00	8.4213 (±0.19)	15.4950 (±0.12)
0.2 % Ir-TiO$_2$	5.3	700	20.00	13.9476 (±0.15)	22.9049 (±0.07)
		750	50.00	14.6913 (±0.12)	24.6717 (±0.29)
0.5 % Ir-TiO$_2$	4.1	700	40.00	13.7592 (±0.08)	21.5960 (±0.16)
		750	80.00	15.3079 (±0.66)	23.3004 (±0.33)
1.0 % Ir-TiO$_2$	2.3	700	40.00	14.2071 (±0.18)	21.6262 (±0.41)
		750	90.00	16.8244 (±0.15)	24.3725 (±0.03)

[a]In the kinetic activity assessment, equilibrium conversion rates were determined in triplicate, with standard deviations reported in parentheses. The reaction gas mixture consisted of CH_4 and CO_2 (20 vol.% CH_4, 20 vol.% CO_2, 1 vol.% N_2, balance Ar).

Supplementary Table 5. Comparison of the as-prepared Ir/TiO$_2$ with reported representative catalytic systems for DRM reaction

| Sample	Gas feed	Tem. (°C)	GHSV (mL·g$_{cat}^{-1}$·h^{-1})	CH$_4$ conv. (%)	CO$_2$ conv. (%)	Average H$_2$/CO	CH$_4$ TOF (s^{-1})	Reaction rate (mol$_{CH_4}$·g$_{metal}^{-1}$·h^{-1})	Ref.
0.05%Ir/TiO$_2$	20%CH$_4$,20%CO$_2$	750	38,760	33	49	0.9	37.25	698	This work
0.5%Ir/TiO$_2$	20%CH$_4$,20%CO$_2$	750	38,760	75	83	0.7	38.84	447	This work
0.6%Ir/CeO$_{2-x}$	44%CH$_4$,44%CO$_2$	650	240,000	57	69	0.8	168	763	[1]
Ir-BaTiO$_3$	2.5%CH$_4$,2.5%CO$_2$	750	267,000	83	87	1.0	-	-	[2]
NiIr/MgAl$_2$O$_4$	50%CH$_4$,50%CO$_2$	750	40,000	85	95	0.9	-	0.75	[3]
NiIr/Mg(Al)O	50%CH$_4$,50%CO$_2$	850	60,000	71	77	0.7	-	-	[4]
Ru$_1$/Mg-CeO$_2$-NR	25%CH$_4$,25%CO$_2$	500	160,000	-	-	0.6	-	-	[5]
Ni$_{90}$Mo$_{10}$/Al$_2$O$_3$	20%CH$_4$,20%CO$_2$	500	20,000	12	20	0.4	-	3.29	[6]
Ni$_{0.1}$Fe$_{0.045}$Rh$_{0.005}$	33%CH$_4$,34%CO$_2$	750	36,000	-	-	-	-	10.11	[7]
Re-Ni$_{0.1}$Fe$_{0.045}$Rh$_{0.005}$	33%CH$_4$,34%CO$_2$	750	36,000	67	78	-	-	16.96	[7]
Ni/SiBeta	33%CH$_4$,34%CO$_2$	750	100,000	76.5	83.2	0.9	8.3	-	[8]
Ni/MgAl$_2$O$_4$	25%CH$_4$,25%CO$_2$	800	160,000	78	84	0.92	-	-	[9]
40cAl-Ni/MgAl$_2$O$_4$	20%CH$_4$,20%CO$_2$	800	60,000	90	95	-	-	-	[10]
5Ni5Co/SiO$_2$	45%CH$_4$,45%CO$_2$	750	24,000	88	91	0.9	-	-	[11]
Ni-MFI-PO	45%CH$_4$,45%CO$_2$	600	62,000	51.6	64.9	0.77	1.44	-	[12]
Rh/CeO$_2$-850-CO$_2$	50%CH$_4$,50%CO$_2$	850	36,000	90	95	1	20.4	384	[13]
0.5Ni$_1$/HAP	20%CH$_4$,20%CO$_2$	750	12 × 10^6	50	60	-	13.3	816.5	[14]
0.5Ni$_1$/HAP-Ce	20%CH$_4$,20%CO$_2$	750	60,000	65	78	0.8	6.1	373.1	[15]
PdNi/MgO	7%CH$_4$,7%CO$_2$	750	70,000	97	96	0.99	-	0.22	[16]
PtNi/Al$_2$O$_3$	20%CH$_4$,20%CO$_2$	700	30,000	69	76	0.65	-	0.18	[17]
RhNiCo/ZrO$_2$/Al$_2$O$_3$	47H$_4$,47%CO$_2$	800	45,000	67.6	71.8	0.84	-	0.63	[18]

Supplementary Table 6. The loading of iridium catalysts determined by ICP-OES analysis

| Sample	Irk loading (%)
0.05%Ir/SiO$_2$	0.01817%
0.05%Ir/Al$_2$O$_3$	0.02840%
0.05%Ir/MgO	0.02826%
0.05% Ir/TiO$_2$-750/4h	0.05883%

Supplementary Figures
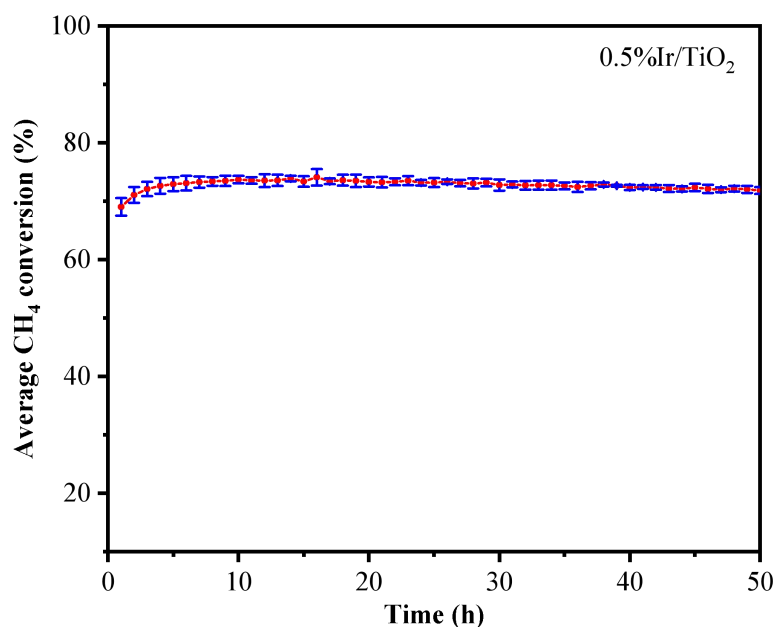
Supplementary Figure 1. Average CH_4 Conversion in the Dry Reforming of Methane (DRM) Reaction. Error bars represent the standard deviation from triplicate experiments using independently prepared catalyst batches. Catalyst loading was maintained consistent across different batches. A gas mixture comprising CH_4 and CO_2 (20 vol.% CH_4, 20 vol.% CO_2, 1 vol.% N_2, Ar balanced) was introduced at a total flow rate of 30 mL/min, corresponding to a gas hourly space velocity (GHSV) of 36,000 $mL \cdot g_{cat}^{-1} \cdot h^{-1}$.
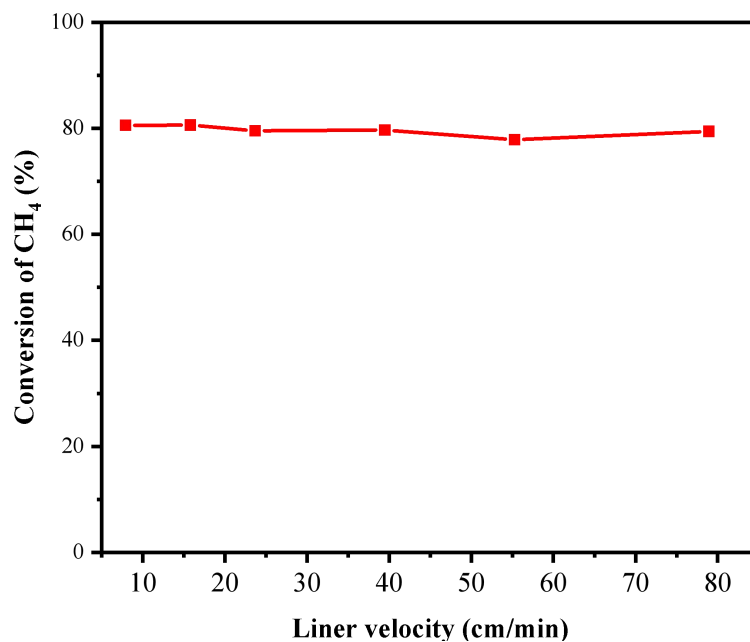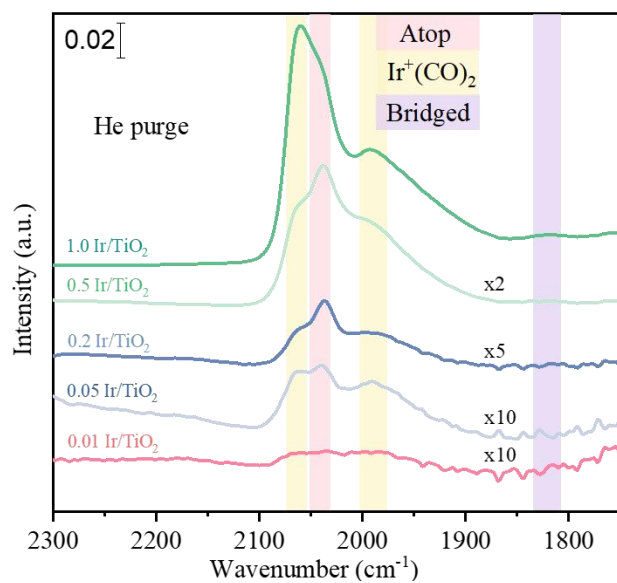
Supplementary Figure 2. Elimination of external diffusion over Ir/TiO$_2$. A gas mixture comprising CH$_4$ and CO$_2$ (20 vol.% CH$_4$, 20 vol.% CO$_2$, 1 vol.% N$_2$, Ar balanced) was introduced at a total flow rate of 30 mL/min, corresponding to a gas hourly space velocity (GHSV) of 36,000 mL·g$_{cat}^{-1}$·h^{-1}.
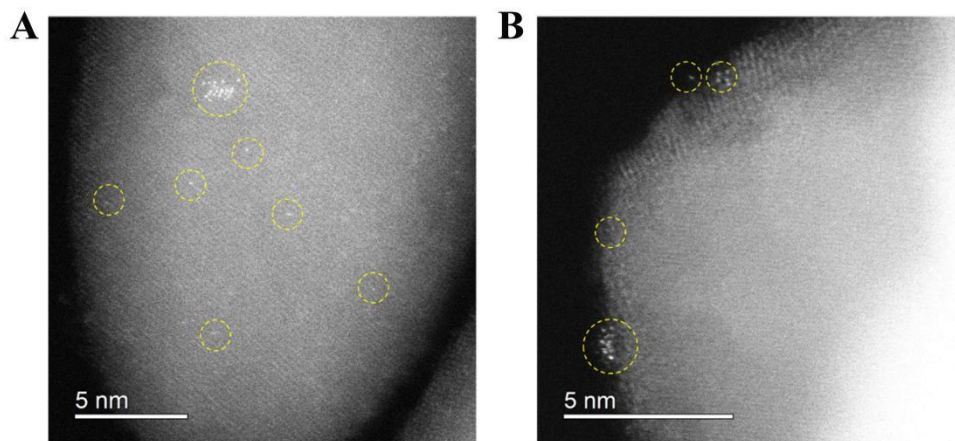
**Supplementary Figure 3.** AC-HADDF-STEM images of 0.05% Ir/TiO$_2$ after reduction at 500 ℃ (A and B).
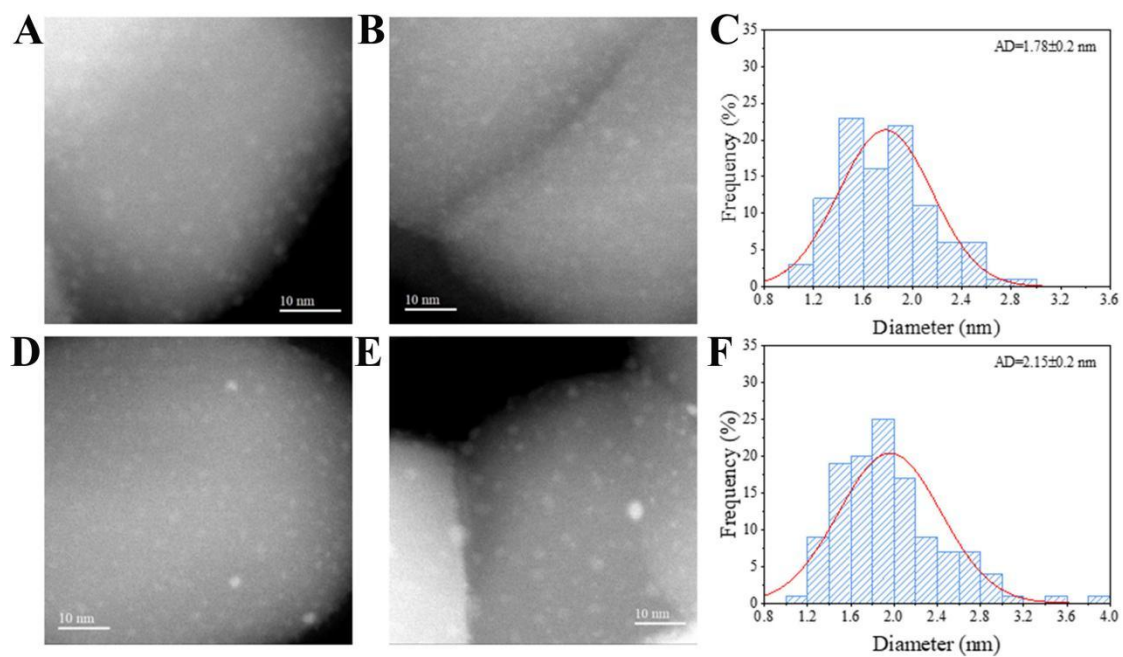
Supplementary Figure 4. STEM images and size distributions of 0.05% Ir/TiO$_2$-750/4h after reduction at 500 ℃ (A-C) and reaction 50 h (D-F).
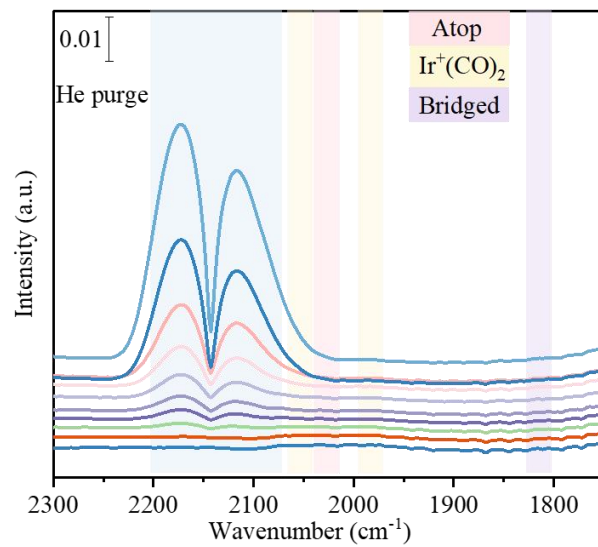
Supplementary Figure 5. *In situ* DRIFT spectra of CO adsorption on 0.01% Ir/TiO$_2$ after reduction at 500 ℃.

Supplementary Figure 6. *In situ* DRIFT spectra of CO adsorption after He purging on Ir/TiO$_2$ with different loadings after reduction at 500 °C.
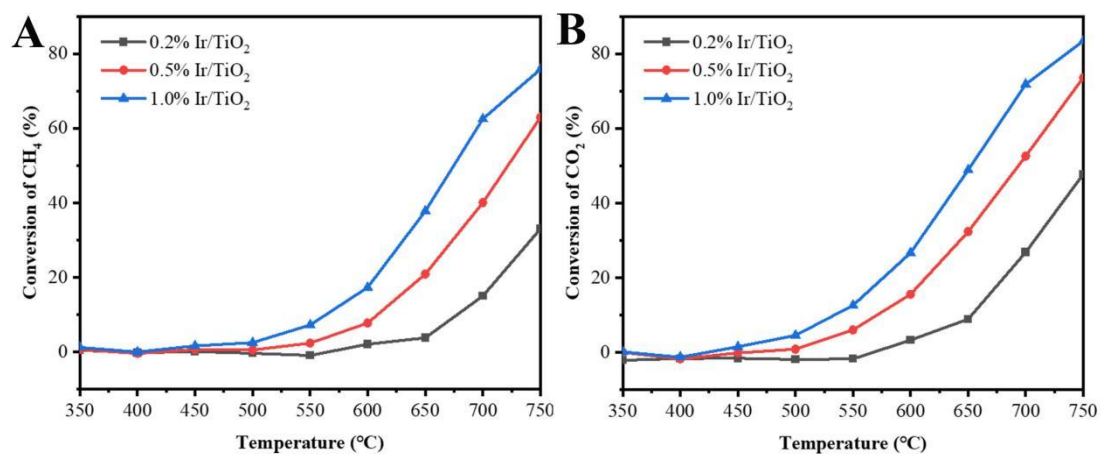
Supplementary Figure 7. Temperature-programmed reaction of 0.2-1.0% Ir/TiO$_2$ catalysts of DRM reaction. The conversion of CH$_4$ (A) and CO$_2$ (B). A gas mixture comprising CH$_4$ and CO$_2$ (20 vol.% CH$_4$, 20 vol.% CO$_2$, 1 vol.% N$_2$, Ar balanced) was introduced at a total flow rate of 30 mL/min, corresponding to a gas hourly space velocity (GHSV) of 36,000 mL·g$_{cat}^{-1}$·h^{-1}.
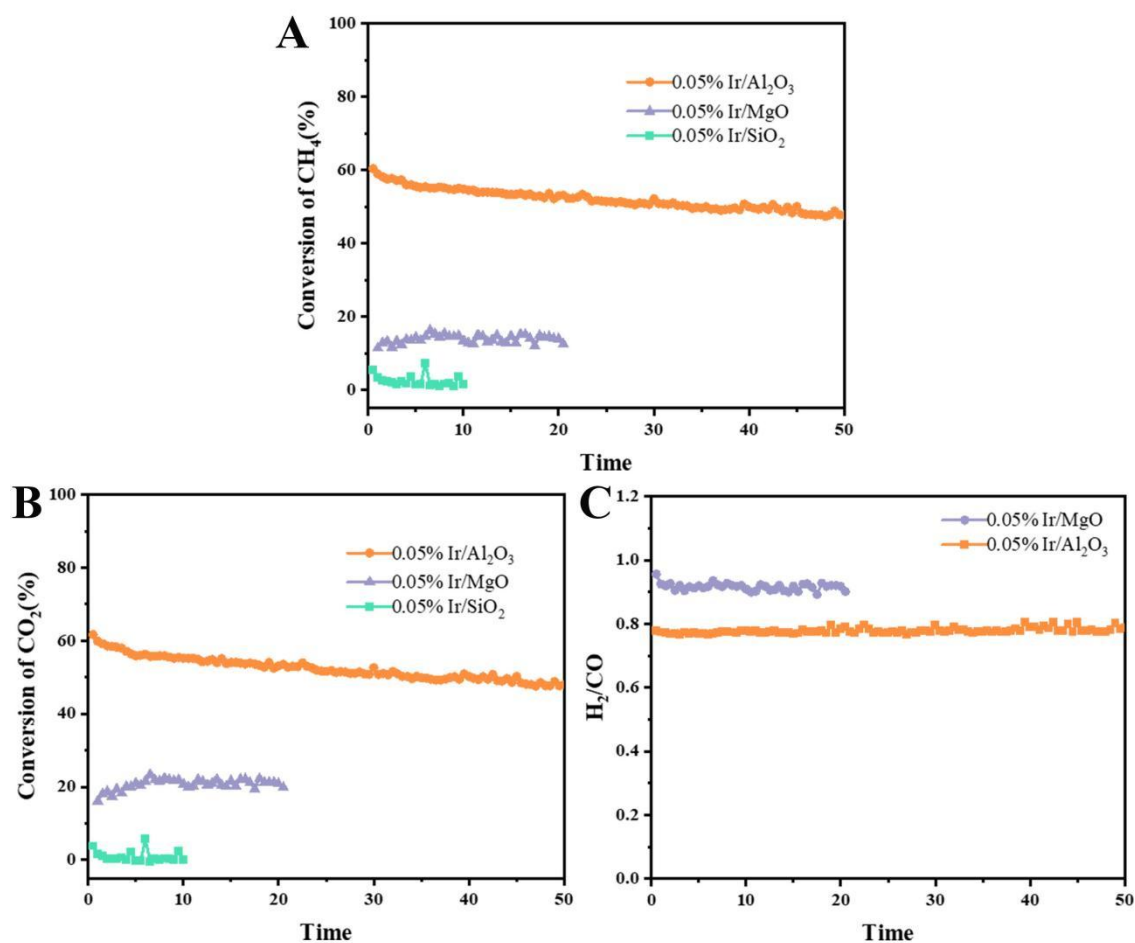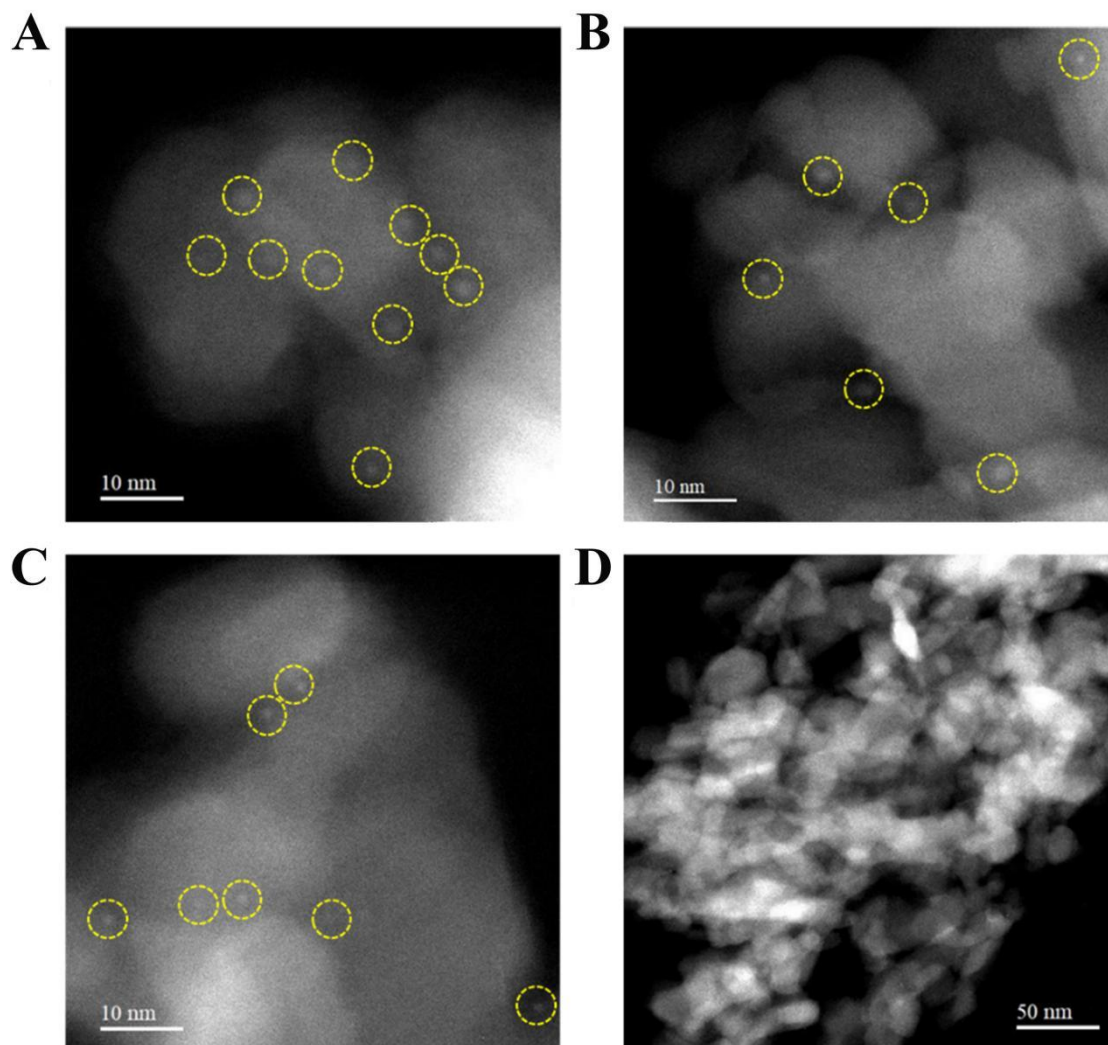
Supplementary Figure 8. The 0.05% Ir/Al_2O_3, Ir/MgO and Ir/SiO_2 catalysts for DRM reaction. (A) CH_4 conversion (B) CO_2 conversion and (C) the ratio of H_2/CO. DRM: Dry reforming of methane. A gas mixture comprising CH_4 and CO_2 (20 vol.% CH_4, 20 vol.% CO_2, 1 vol.% N_2, Ar balanced) was introduced at a total flow rate of 30 mL/min, corresponding to a gas hourly space velocity (GHSV) of 36,000 $mL \cdot g_{cat}^{-1} \cdot h^{-1}$.
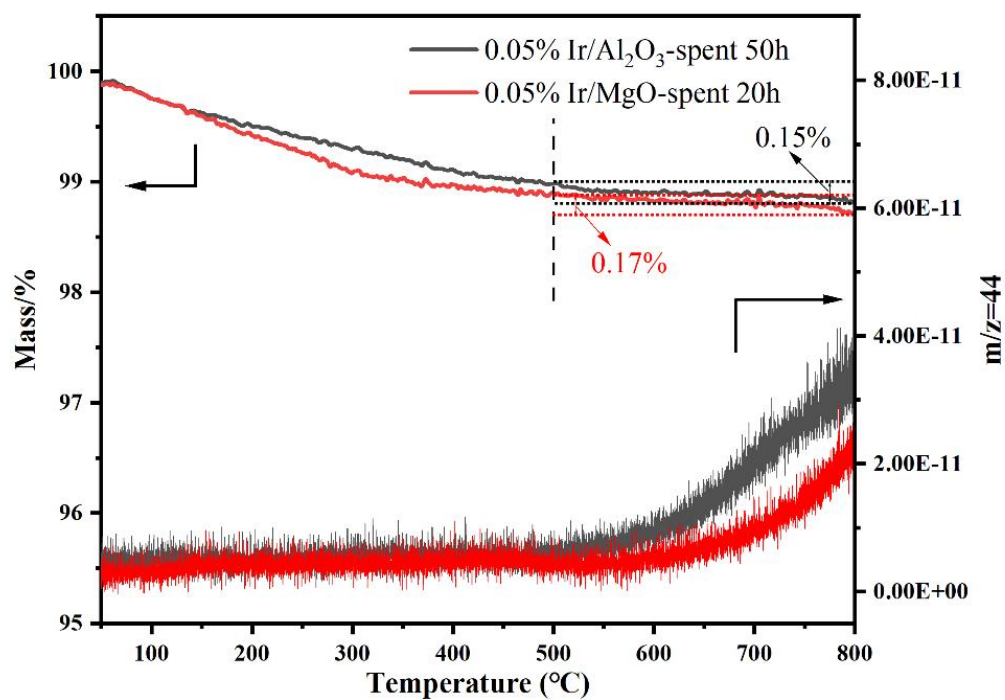
Supplementary Figure 9. TGA-MS profiles of 0.05%Ir/Al$_2$O$_3$-spent 50 h and 0.05%Ir/MgO-spent 20 h catalysts after DRM reaction.

Supplementary Figure 10. STEM images of 0.05% Ir/Al_2O_3 after reaction for 50 h. (A-C) The high magnification images of 0.05% Ir/Al_2O_3; (D) The low magnification images of 0.05% Ir/Al_2O_3.
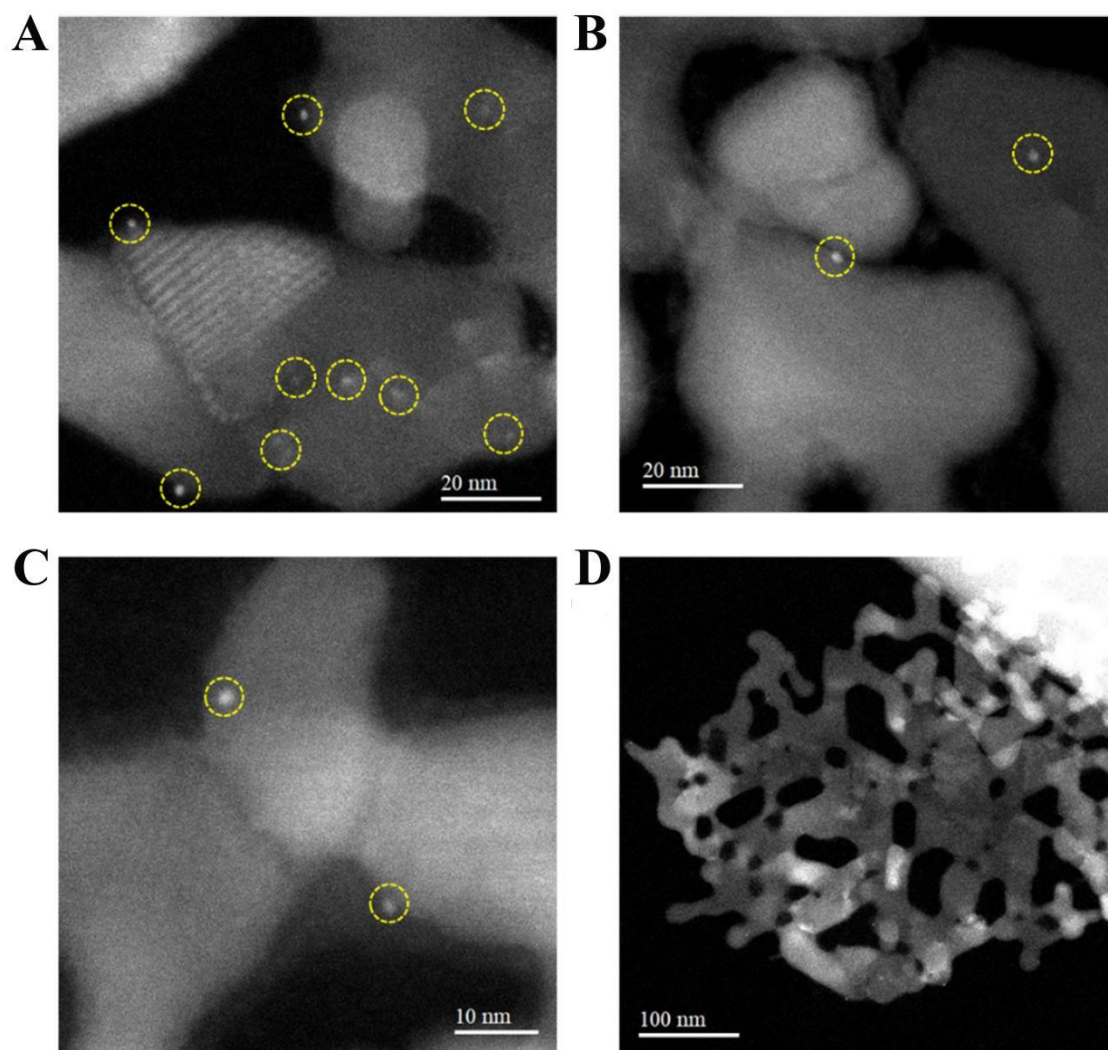
Supplementary Figure 11. STEM images of 0.05% Ir/MgO after reaction for 20 h. (A-C) The high magnification images of 0.05% Ir/MgO; (D) The low magnification image of 0.05% Ir/ MgO.
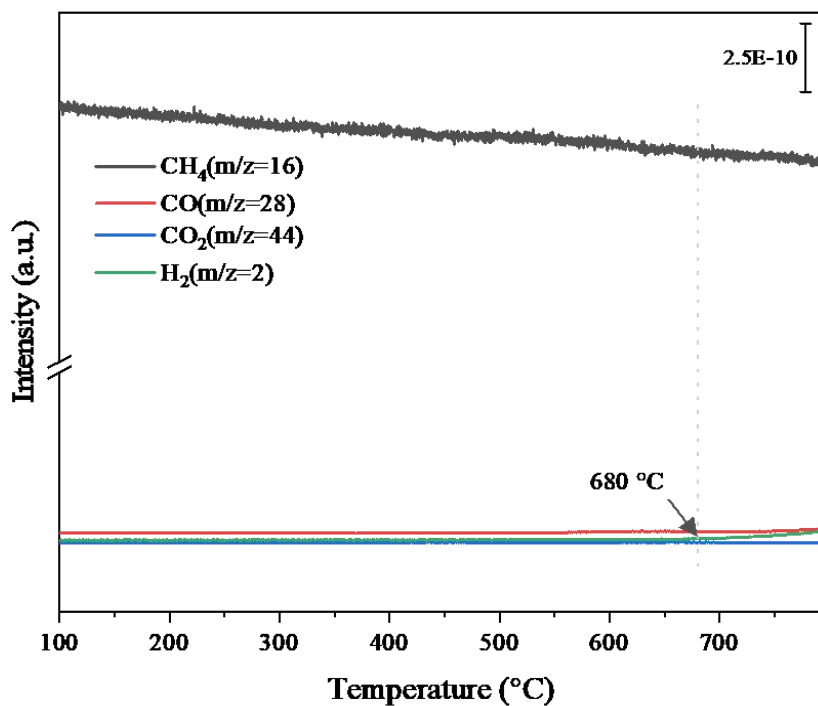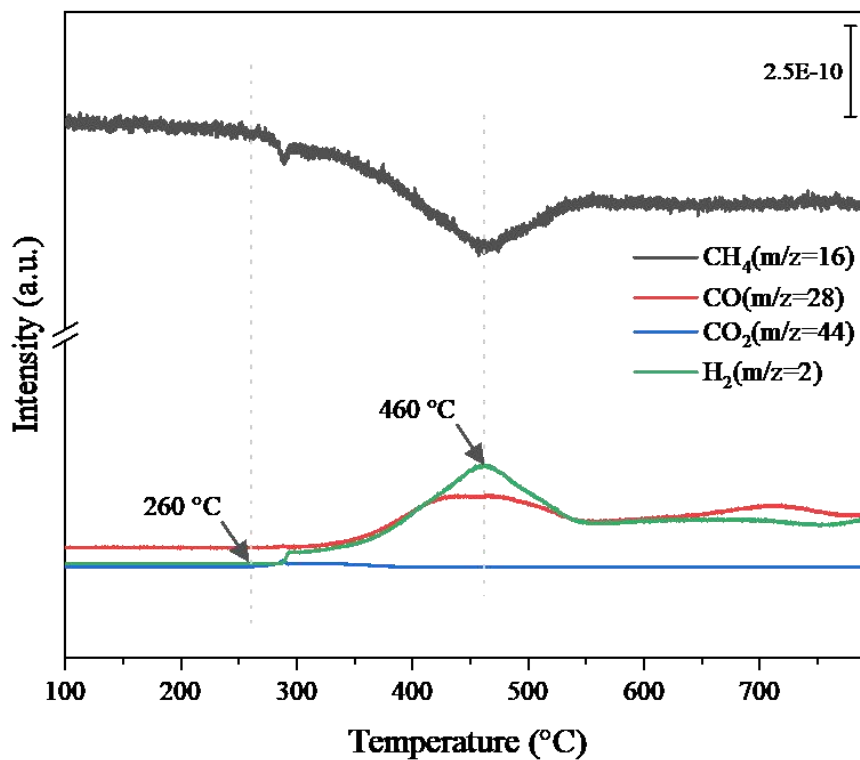
Supplementary Figure 12. Mass spectrometer signals of CH_4, CO_2, CO and H_2 during the CH_4-TPSR experiment over TiO_2 support. The mixture gas is 1 vol%CH_4 balanced with He.
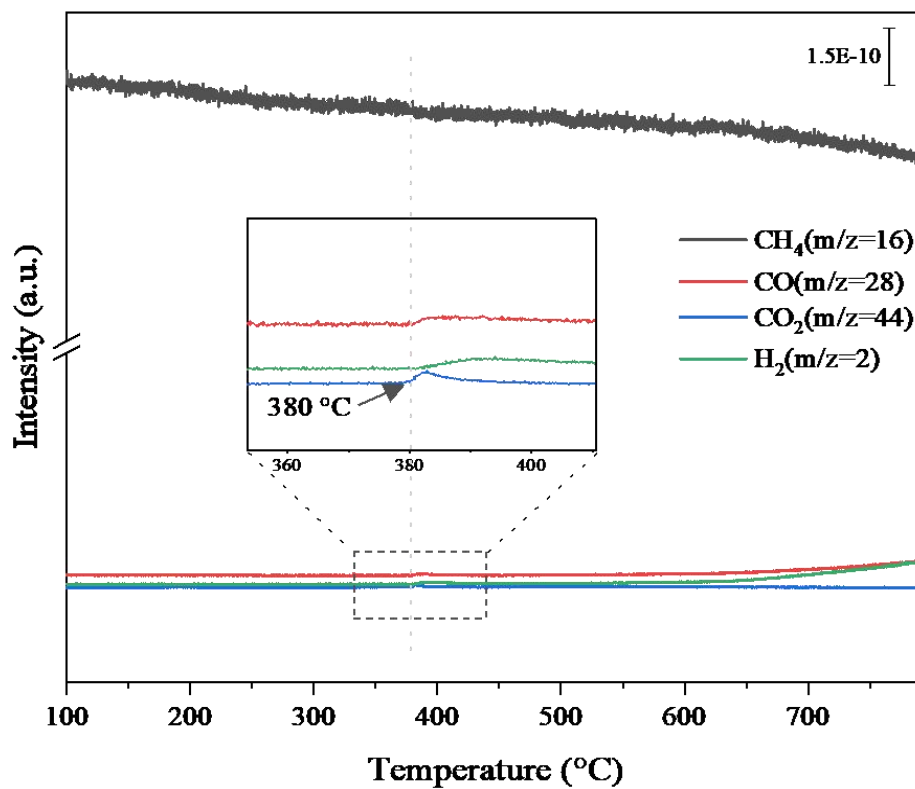
Supplementary Figure 13. Mass spectrometer signals of CH_4, CO_2, CO and H_2 during the CH_4-TPSR experiment over 0.01% Ir/TiO_2. The mixture gas is 1 vol%CH_4 balanced with He.
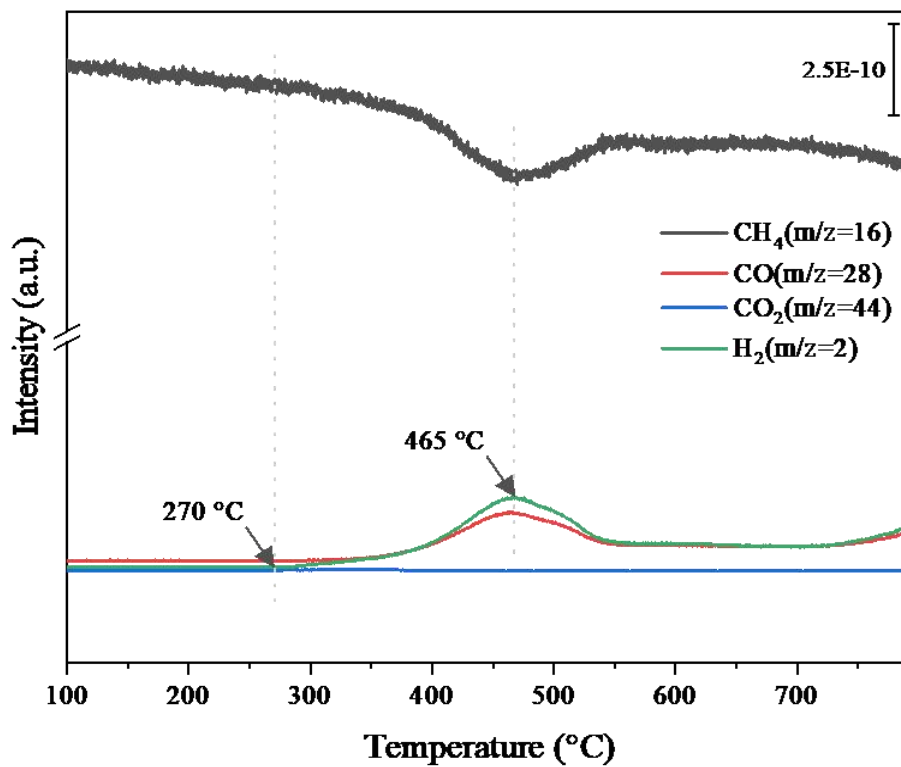
Supplementary Figure 14. Mass spectrometer signals of CH_4, CO_2, CO and H_2 during the CH_4-TPSR experiment over 0.2% Ir/TiO_2. The mixture gas is 1 vol%CH_4 balanced with He.
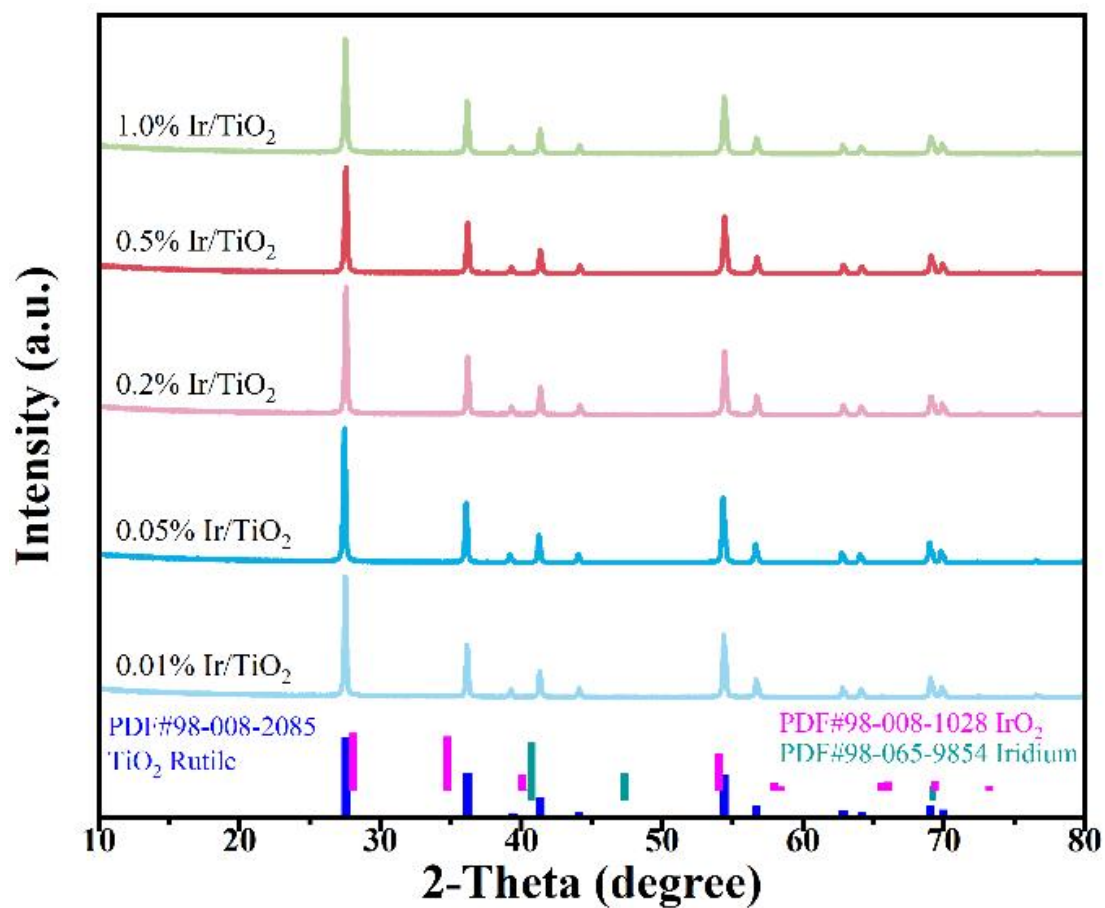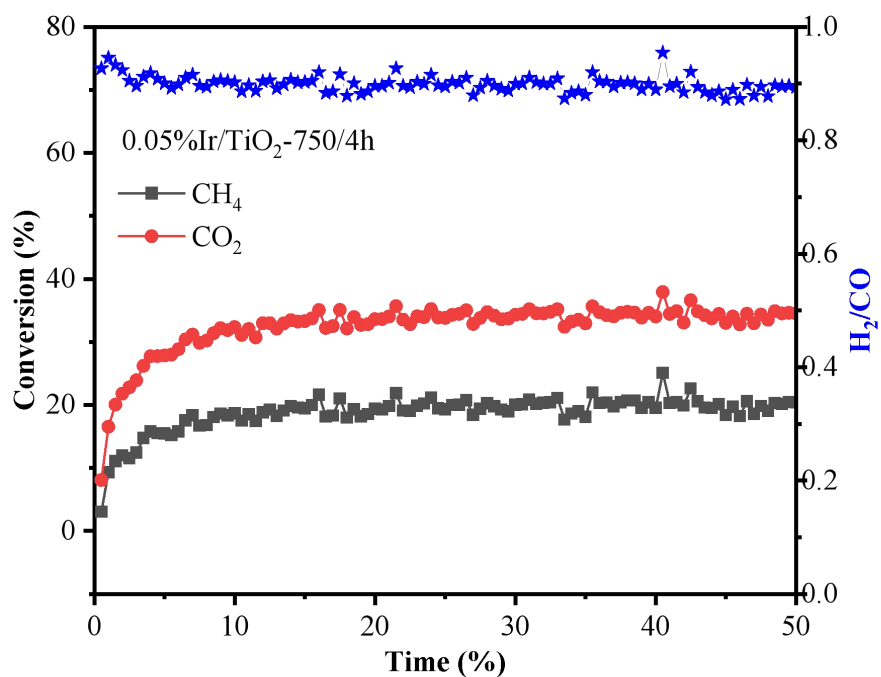
Supplementary Figure 15. Mass spectrometer signals of CH_4, CO_2, CO and H_2 during the CH_4-TPSR experiment over 0.5% Ir/TiO_2. The mixture gas is 1 vol%CH_4 balanced with He.

Supplementary Figure 16. XRD patterns of different loading Ir/TiO$_2$ catalysts after dry reforming of methane (DRM) reaction for 50 h.

Supplementary Figure 17. The DRM reaction of 0.05%Ir/TiO₂-750/4h. A gas mixture comprising CH_4 and CO_2 (20 vol.% CH_4, 20 vol.% CO_2, 1 vol.% N_2, Ar balanced) was introduced at a total flow rate of 30 mL/min, corresponding to a gas hourly space velocity (GHSV) of 36,000 $mL·g_{cat}^{-1}·h^{-1}$.
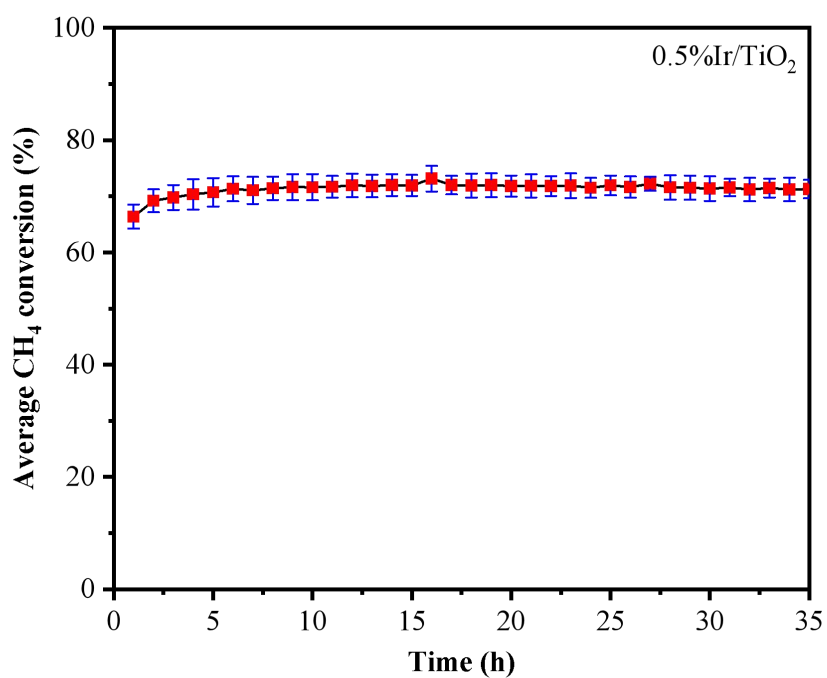
Supplementary Figure 18. Average CH_4 Conversion in the Dry Reforming of Methane (DRM) Reaction. Error bars represent the standard deviation from triplicate experiments using the same batch catalyst. A gas mixture comprising CH_4 and CO_2 (20 vol.% CH_4, 20 vol.% CO_2, 1 vol.% N_2, Ar balanced) was introduced at a total flow rate of 30 mL/min, corresponding to a gas hourly space velocity (GHSV) of 36,000 $mL \cdot g_{cat}^{-1} \cdot h^{-1}$.

REFERENCES

1. Wang H, Cui G, Lu H, et al. Facilitating the dry reforming of methane with interfacial synergistic catalysis in an Ir@CeO$_{2-x}$ catalyst. *Nature Communications* 2024;15. http://dx.doi.org/10.1038/s41467-024-48122-6

2. Cali E, Saini S, Kerherve G, et al. Enhanced Stability of Iridium Nanocatalysts via Exsolution for the CO$_2$ Reforming of Methane. *ACS Applied Nano Materials* 2023.http://dx.doi.org/10.1021/acsanm.3c04126

3. Li H, Hao C, Tian J, Wang S, Zhao C. Ultra-durable Ni-Ir/MgAl$_2$O$_4$ catalysts for dry reforming of methane enabled by dynamic balance between carbon deposition and elimination. *Chem Catalysis* 2022;2:1748-63. http://dx.doi.org/10.1016/j.checat.2022.05.005

4. Huang Y, Li X, Zhang Q, Vinokurov VA, Huang W. Enhanced carbon tolerance of hydrotalcite-derived Ni-Ir/Mg(Al)O catalysts in dry reforming of methane under elevated pressures. *Fuel Processing Technology* 2022;237. http://dx.doi.org/10.1016/j.fuproc.2022.107446

5. Zhang Z-Y, Huang Z-X, Yu X-Y, et al. Photo-thermal coupled single-atom catalysis boosting dry reforming of methane beyond thermodynamic limits over high equivalent flow. *Nano Energy* 2024;123. http://dx.doi.org/10.1016/j.nanoen.2024.109401

6. Zhou C, Zhang Y, Li B, Yang B, Li L. Resolving the Active Role of Isolated Transition Metal Species in Ni-Based Catalysts for Dry Reforming of Methane. *ACS Catalysis* 2024;14:4164-74. http://dx.doi.org/10.1021/acscatal.3c05737

7. Yao X, Cheng Q, Bai X, et al. Enlarging the Three-Phase Boundary to Raise CO$_2$/CH$_4$ Conversions on Exsolved Ni–Fe Alloy Perovskite Catalysts by Minimal Rh Doping. *ACS Catalysis* 2024;14:5639-53. http://dx.doi.org/10.1021/acscatal.4c00151

8. He D, Wu S, Cao X, et al. Dynamic trap of Ni at elevated temperature for yielding high-efficiency methane dry reforming catalyst. *Applied Catalysis B: Environmental* 2024;346. http://dx.doi.org/10.1016/j.apcatb.2024.123728

9. Feng K, Zhang J, Li Z, et al. Spontaneous regeneration of active sites against catalyst deactivation. *Applied Catalysis B: Environmental* 2024;344. http://dx.doi.org/10.1016/j.apcatb.2023.123647

10. Cai L, Han S, Xu W, Chen S, Shi X, Lu J. Formation of a Porous Crystalline Mg$_{1-x}$Al$_2$O$_y$ Overlayer on Metal Catalysts via Controlled Solid-State Reactions for High-temperature Stable Catalysis. *Angewandte Chemie International Edition* 2024. http://dx.doi.org/10.1002/anie.202404398

11. Zou Z, Zhang T, Lv L, et al. Preparation adjacent Ni-Co bimetallic nano catalyst for dry reforming of methane. *Fuel* 2023;343. http://dx.doi.org/10.1016/j.fuel.2023.128013

12. Cheng Q, Yao X, Ou L, et al. Highly Efficient and Stable Methane Dry Reforming Enabled by a Single-Site Cationic Ni Catalyst. *Journal of the Amercian Chemical Society* 2023, 145:25109-19 http://dx.doi.org/10.1021/jacs.3c04581

13. Gangarajula Y, Hong F, Li Q, et al. Operando induced strong metal-support

interaction of Rh/CeO$_2$ catalyst in dry reforming of methane. *Applied Catalysis B-Environment and Energy* 2024;343:9. http://dx.doi.org/10.1016/j.apcatb.2023.123503

14. Akri M, El Kasmi A, Batiot-Dupeyrat C, Qiao B. Highly active and carbon-resistant nickel single-atom catalysts for methane dry reforming. *Catalysts* 2020;10:20. http://dx.doi.org/10.3390/catal10060630

15. Akri M, Zhao S, Li X, et al. Atomically dispersed nickel as coke-resistant active sites for methane dry reforming. *Nature Communications* 2019;10:5181. http://dx.doi.org/10.1038/s41467-019-12843-w

16. Singha RK, Shukla A, Sandupatla A, Deo G, Bal R. Synthesis and catalytic activity of a Pd doped Ni–MgO catalyst for dry reforming of methane. *Journal of Materials Chemistry A* 2017;5:15688-99. http://dx.doi.org/10.1039/c7ta04452f

17. García-Diéguez M, Pieta IS, Herrera MC, Larrubia MA, Alemany LJ. Nanostructured Pt- and Ni-based catalysts for CO$_2$-reforming of methane. *Journal of Catalysis* 2010;270:136-45. http://dx.doi.org/10.1016/j.jcat.2009.12.010

18. Al-Fatesh A, Singh SK, Kanade GS, et al. Rh promoted and ZrO$_2$/Al$_2$O$_3$ supported Ni/Co based catalysts: High activity for CO$_2$ reforming, steam–CO$_2$ reforming and oxy–CO$_2$ reforming of CH$_4$. *International Journal of Hydrogen Energy* 2018;43:12069-80. http://dx.doi.org/10.1016/j.ijhydene.2018.04.152